

Experimental quantum advantage with quantum coupon collector

Min-Gang Zhou,^{1,*} Xiao-Yu Cao,^{1,*} Yu-Shuo Lu,^{1,*} Yang Wang,¹ Yu Bao,¹ Zhao-Ying Jia,¹ Yao Fu,² Hua-Lei Yin,^{1,†} and Zeng-Bing Chen^{1,2,‡}

¹*National Laboratory of Solid State Microstructures, School of Physics,
Collaborative Innovation Center of Advanced Microstructures, Nanjing University, Nanjing 210093, China*

²*MatrixTime Digital Technology Co. Ltd., Nanjing 211899, China*

(Dated: December 16, 2021)

An increasing number of communication and computational schemes with quantum advantages have recently been proposed, which implies that quantum technology has fertile application prospects. However, demonstrating these schemes experimentally continues to be a central challenge because of the difficulty in preparing high-dimensional states or highly entangled states. In this study, we introduce and analyse a quantum coupon collector protocol by employing coherent states and simple linear optical elements, which was successfully demonstrated using realistic experimental equipment. We showed that our protocol can significantly reduce the number of samples needed to learn a specific set compared with the classical limit of the coupon collector problem. We also discuss the potential values and expansions of the quantum coupon collector by constructing a quantum blind box game. The information transmitted by the proposed game also broke the classical limit. These results strongly prove the advantages of quantum mechanics in machine learning and communication complexity.

The ‘second quantum revolution’ aims to explore the superiority of quantum resources over classical resources in terms of communication, computation, and artificial intelligence. To demonstrate that this goal is feasible in practice, a series of schemes with quantum advantages were experimentally implemented. These schemes included improving on the security of communication [1–12], enhancing computational power for specific tasks [13–27] and reducing the necessary resources used to complete specific communication tasks [28–33]. In addition, machine learning can extract useful knowledge from data, which can then have a significant impact on productivity, technology, and the economy [34]. This has led to an increasing interest to the question in quantum machine learning [35]: Can we improve machine learning by using quantum resources? Owing to the unique entanglement properties of quantum states, quantum models may be able to produce atypical patterns that cannot be effectively produced by classical models or effectively reduce training time. Therefore, some studies have made bold attempts. For example, in Ref. [36], a quantum autoencoder that can successfully denoise specific quantum states subjected to specific noises were developed. Reference [37] described a quantum neural network that can accurately recognize quantum states associated with a one-dimensional symmetry-protected topological phase. Moreover, there are several other excellent studies [38–46].

On the other hand, most of these attempts are heuristic and have not theoretically prove that quantum machine learning exhibits a better performance or shorter training time than classical machine learning. The training time

of a model includes the time complexity of the learning algorithm. If the algorithm takes a constant amount of time for processing each sample, the concern for the time complexity translates into a concern of the sample complexity. Probably approximately correct (PAC) learning theory [47, 48] provides the minimum number of samples necessary for a learning algorithm to complete a learning task. Researching quantum machine learning using this theory can therefore lay a positive theoretical foundation for exploring quantum advantages in machine learning.

For the first time, Ref. [49] described the use of PAC learning theory to rigorously prove that quantum technology can provide a learning algorithm with quantum advantage for machine learning. The method applied clever quantum measurements to the learning task known as the ‘coupon collector problem’ [50]. Specifically, Ref. [49] gives a surprising result: for the coupon collector problem, the sample complexity of the quantum learning algorithm does not change with changes in the search space of the algorithm. This result is impossible in classical machine learning [47]. However, the experimental demonstration of this algorithm [49] requires high-dimensional states that are difficult to prepare. Even if these states are decomposed into a tensor product of qubits, these qubits must be highly entangled [28, 51, 52]. These requirements are far beyond the scope of current technology. More seriously, the algorithm requires a specific projective measurement, which is difficult to implement in experiment.

In this work, we experimentally demonstrate the quantum coupon collector algorithm by proposing a coherent-state quantum coupon collector protocol. Our protocol avoids the above-mentioned difficulties. To do this, our protocol not only maintains the important properties of the original one, but also introduces new conceptual tools that can be implemented using only linear optics operations and single-photon detectors. Even without a quan-

* These authors contributed equally to this work

† hlyin@nju.edu.cn

‡ zbchen@nju.edu.cn

tum computer, these tools enable us to demonstrate the quantum advantages in machine learning at the current technological level. Moreover, the coupon collector problem can be considered as a communication task. Similar to quantum fingerprinting [29, 30], our protocol also experimentally demonstrates the advantages of quantum mechanics in the context of communication complexity. These results, in addition to their fundamental interest [53–55], will further inspire new designs of communication systems, large-scale integration circuit designs, and data structures [56], thus paving the way for other communication or computational tasks that rely on similar principles.

Results

Coherent-state quantum coupon collector protocol. To clearly describe our protocol, we briefly introduce the coupon collector problem [50]. This problem can be abstracted as learning exactly an unknown set S . Specifically, this set S is limited to a subset of the set $[n] := \{1, \dots, n\}$, where the size k ($k < n$) of set S is known. To learn the set S , several copies of S are given, and only one element is allowed to be extracted from each copy. The task is to determine the minimum number of copies required to learn S exactly.

Because the elements in S are independent of each other, the best strategy for learning S is to randomly extract one of these elements in each copy. Under this strategy, if i ($i < k$) distinct elements have been obtained, the expected number of copies needed to learn the $(i+1)$ th element is $k/(k-i)$. Therefore, the expected number of copies needed to learn S is $\sum_{i=0}^{k-1} \frac{k}{k-i} \sim k \ln k$. Continuing based on this, Ref. [50] shows that $\Theta(k \log_2 k)$ copies are necessary and sufficient for learning S with a high probability.

However, if these copies are quantum copies in the form of $|S\rangle := \frac{1}{\sqrt{k}} \sum_{i \in S} |i\rangle$, the number of copies required can be further reduced. This is because we can perform more quantum operations on $|S\rangle$ before measuring them on a computational basis. In other words, by using quantum copies $|S\rangle$, the strategy for learning S is no longer limited to random sampling. Reference [49] shows that when the number of missing elements $m = n - k$ is very small, the number of copies of $|S\rangle$ used to learn S is reduced to $\Theta(k \log_2(m+1))$. The method first performs a 2-outcome projective measurement with operators $|\langle n|\langle n|$ and $I - |\langle n|\langle n|$ on copies of $|S\rangle$, where $|\langle n| := \frac{1}{\sqrt{n}} \sum_{i \in [n]} |i\rangle$. After the measurement, the second outcome $|\psi\rangle = \sqrt{\frac{m}{n}}|S\rangle - \sqrt{\frac{k}{n}}|\bar{S}\rangle$ is obtained with probability m/n , where \bar{S} is the set of missing elements, and $|\bar{S}\rangle := \frac{1}{\sqrt{m}} \sum_{i \in \bar{S}} |i\rangle$. Then, $|\psi\rangle$ is measured on a computational basis to obtain the missing elements. This method transforms $|S\rangle$ into $|\psi\rangle$, and then infers the elements in $|S\rangle$ by learning the elements in $|\bar{S}\rangle$ from $|\psi\rangle$. Because $|\bar{S}\rangle$ has fewer elements, this method reduces the number of copies required to learn S .

However, difficulties arise when we attempt to demon-

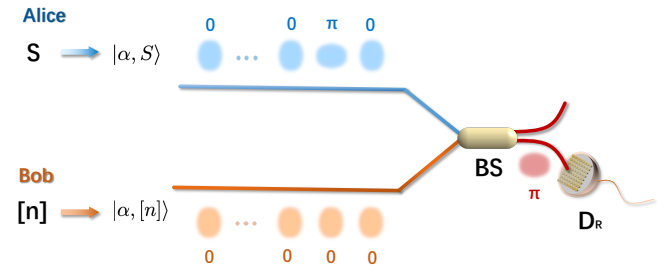


FIG. 1. Coherent-state quantum coupon collector protocol. Alice and Bob generate pulses $|\alpha, S\rangle$ and $|\alpha, [n]\rangle$ according to S and $[n]$, respectively. The pulses travel along their respective routes to interfere at the beam splitter (BS) and are then detected by a single-photon detector D_R . After the experiment, Bob learns the elements in set S according to the results of D_R .

strate this method experimentally. This is because it is difficult to experimentally construct a single k -dimensional quantum state [57–59]. Even if this state is decomposed into a tensor product of qubits, these qubits must be highly entangled [28, 51, 52]. This is also not feasible using current technology. More seriously, the operators $|\langle n|\langle n|$ and $I - |\langle n|\langle n|$ in this method are difficult to implement in experiment. Therefore, we introduce an alternative scheme, which is defined as ‘coherent-state quantum coupon collector protocol’. This scheme maintains the main idea of the original one, which is to learn S by measuring the missing elements. In addition, this scheme uses a sequence of coherent states to implement copies of $|S\rangle$. Coherent states are easy to prepare and can be transformed using simple linear optical elements. Therefore, this scheme is particularly attractive from a practical point of view.

In our scheme, copies of $|S\rangle$ are implemented using a time sequence of n weak coherent optical pulses

$$|\alpha, S\rangle := \bigotimes_{i=1}^n |(-1)^j \alpha\rangle_i, \quad (1)$$

where α is a complex number, and $|(-1)^j \alpha\rangle_i$ is a coherent state with amplitude α at the i th time mode, where $j = 0$ for $i \in S$ and $j = 1$ otherwise. The phases of these coherent pulses depend on S , but their intensities are the same. Thus, the state $|\alpha, S\rangle$ has the mean photon number $\mu = n|\alpha|^2$. Note that $|S\rangle$ is given by projecting the state $|\bar{\alpha}, S\rangle := \bigotimes_{i \in S} |\alpha\rangle_i$ into the single-photon subspace. The total intensity $k|\alpha|^2$ of $|\bar{\alpha}, S\rangle$ represents the number of copies of $|S\rangle$. However, our scheme uses $|\alpha, S\rangle$ instead of $|\bar{\alpha}, S\rangle$. In other words, when $i \notin S$, our scheme sends state $|\alpha\rangle_i$ instead of a vacuum state. This method can improve the efficiency of detecting missing elements, but it also causes the number of copies by our scheme to be slightly different from those of a scheme using $|\bar{\alpha}, S\rangle$. Specifically, the number of copies by our scheme are at most $O(n|\alpha|^2)$. For comparison, the number of copies by a scheme using $|\bar{\alpha}, S\rangle$ are at most $O(k|\alpha|^2)$. However, as

we will see later, this subtle difference can be ignored, and using $|\alpha, S\rangle$ greatly improves the efficiency of detecting missing elements.

As we discussed previously, our scheme maintains the important characteristics of the original one, that is, the time step i of state $|- \alpha\rangle_i$ in $|\alpha, S\rangle$ is found through complementary measurements, and the elements in S are derived from these time steps. To do this, a local state $|\alpha, [n]\rangle$ is prepared and sent to a 50 : 50 beam splitter (BS) to interfere with $|\alpha, S\rangle$ (Fig. 1), where

$$|\alpha, [n]\rangle := \bigotimes_{i=1}^n |\alpha\rangle_i. \quad (2)$$

The interference result is recorded by a single photon detector D_R . If the detector D_R clicks at the i th time step, then we consider the pulse of the i th time step in $|\alpha, S\rangle$ to be $|- \alpha\rangle_i$. Thus, all time steps containing $|- \alpha\rangle$ in $|\alpha, S\rangle$ can be learned exactly from the outcomes of the detector D_R . The detailed steps are described as follows.

(1) Alice selects k elements from set $[n]$ as set S and selects an appropriate value $|\alpha|^2$ as the intensity of each pulse.

(2) Alice encodes the pulses $|\alpha, S\rangle$ according to S and the intensity $|\alpha|^2$; if $i \in S$, Alice prepares a coherent pulse $|\alpha\rangle_i$ at the i th time step and sends it to Bob; otherwise, Alice sends $|- \alpha\rangle_i$ to Bob.

(3) Alice announces the value of $|\alpha|^2$, the elements of $[n]$, and the size k of S .

(4) Bob encodes the pulses $|\alpha, [n]\rangle$ according to $[n]$ and intensity $|\alpha|^2$: Bob prepares a coherent pulse $|\alpha\rangle$ for all time steps.

(5) Bob uses a 50 : 50 beam splitter and two single-photon detectors to perform interference measurements on the pulses $|\alpha, S\rangle$ and $|\alpha, [n]\rangle$.

(6) Bob records whether the detector D_R clicks or not at each time step, and then learns S exactly based on the outcomes of the detector D_R and the size k of the set S .

However, even under ideal conditions, the proposed scheme has an intrinsic failure probability. This is because a coherent pulse may collapse to a vacuum state after being measured, and thus, cannot be detected by detector D_R . Specifically, when Alice sends the coherent pulse $|\alpha\rangle_i$, D_R will never click. Therefore, Bob can always obtain the correct results. However, when Alice sends a coherent pulse $|- \alpha\rangle_i$, the detector D_R has a non-click probability of $P_{\text{not}} = e^{-2|\alpha|^2}$. Note that if Alice sends a vacuum state when $i \notin S$, then the non-click probability of D_R is increased to $e^{-\frac{|\alpha|^2}{2}}$. This is why when $i \notin S$, our scheme sends $|- \alpha\rangle_i$ instead of a vacuum state. Only when detector D_R detects all $|- \alpha\rangle_i$ sent by Alice can we infer the elements in S . Therefore, the success probability of our scheme without experimental imperfections is $P(m) = (1 - P_{\text{not}})^m$, where m is the number of missing elements of S . Note that although the use of the coherent state sequence $|\alpha, S\rangle$ for implementing copies of $|S\rangle$ is easier to demonstrate experimentally, it also introduces

an intrinsic failure probability. Fortunately, as we will see later, this failure probability is negligible compared to the failure probability introduced by experimental imperfections.

To demonstrate the quantum advantage of our scheme experimentally, we need to eliminate the influence of the failure probability as much as possible. On the one hand, we can reduce the failure probability by increasing the mean photon number per coherent pulse. On the other hand, we can calculate the required number of copies based on the expectation of 100% success. However, these methods increase the number of copies required. Therefore, the selection of an appropriate mean photon number is particularly important.

Protocol in the presence of experimental imperfections. So far, we have only discussed the success probability of our protocol under ideal conditions. However, owing to experimental imperfections, the success probability formula of our protocol must be modified. We consider imperfect experimental models characterised by three parameters: the combined effects of limited detector efficiency and channel loss η , dark counts p_d of the single-photon detector, and the limited visibility ν of the interferometer.

By replacing $|\alpha, S\rangle$ with $|\sqrt{\eta}\alpha, S\rangle$ can eliminate the effect of η without changing the form of the success probability formula. However, p_d and ν will cause D_R to click at incorrect time steps with a non-zero probability; thus, the success probability formula must be modified. In this case, when Alice sends a pulse $|\alpha\rangle_i$, the probability that detector D_R clicks is given by

$$P_\alpha = \left(1 - e^{-2(1-\nu)|\alpha|^2\eta}\right) + p_d, \quad (3)$$

and when Alice sends a pulse $|- \alpha\rangle_i$, the probability that the detector D_R clicks is

$$P_{-\alpha} = \left(1 - e^{-2|\alpha|^2\eta}\right) + p_d. \quad (4)$$

Because D_R may click when Alice sends $|\alpha\rangle_i$ and may not click when Alice sends $|- \alpha\rangle_i$, the number of clicks of the detector D_R may be different from the size k of S . In this case, Bob can determine that the experimental results are not available and must be discarded. Therefore, Alice and Bob need to repeat multiple experiments to obtain usable experimental data. Here, we define a new efficiency $E = M/N$ to measure the ratio of the number M of available experimental results of the total number N of experiments, which can be calculated by the following formula:

$$E = \sum_{i=0}^m D_{-\alpha}^{mi} D_\alpha^{k(m-i)} \quad (5)$$

where $D_{-\alpha}^{mi} = C_m^i P_{-\alpha}^i (1 - P_{-\alpha})^{m-i}$ represents the sum of the probabilities of all possible cases where D_R detects i out of m coherent states $|- \alpha\rangle$ sent by Alice, and

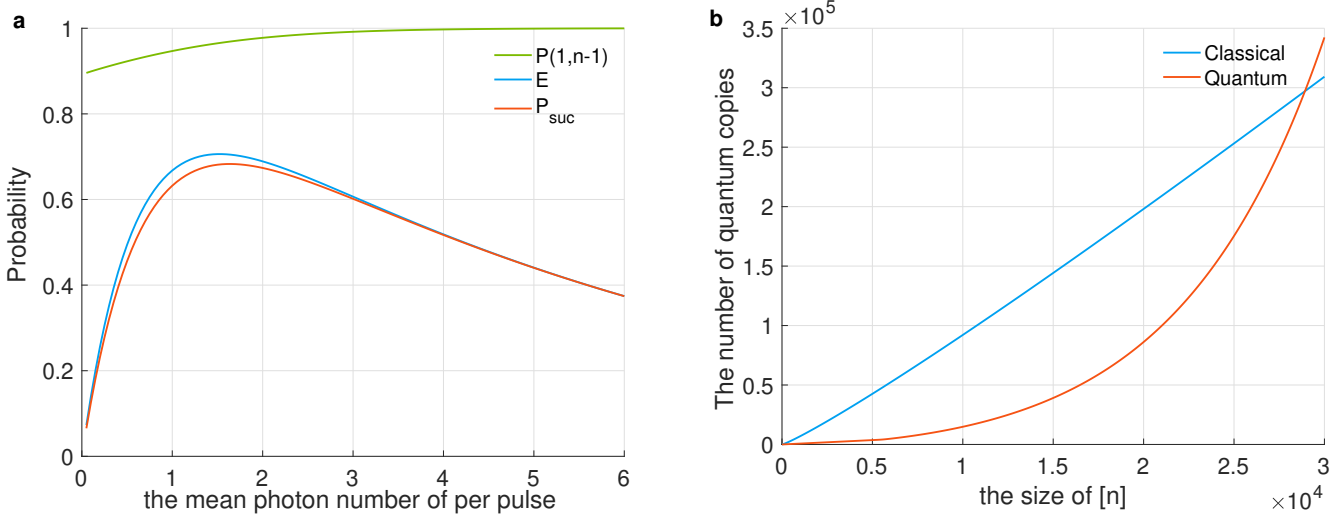


FIG. 2. Numerical results. (a) Efficiency E , correct probability $P(1, n - 1)$ and success probability P_{suc} versus different mean photon numbers per pulse. We draw the numerical results under $n = 4000$, $k = n - 1$, $p_d = 10^{-8}$, $\nu = 0.99998$, and $\eta = 68\%$. (b) The required samples for the classical and quantum protocols versus the size of the set $[n]$ with $p_d = 10^{-8}$, $\nu = 0.99998$, and $\eta = 68\%$.

TABLE I. Experimental parameters corresponding to our numerical simulation and experimental demonstration. Note that the channel loss η is split into channel efficiency η_{cha} and detector efficiency η_{det} . Here p_d is dark counts of the single-photon detector and ν is the limited visibility of the interferometer.

η_{cha}	η_{det}	p_d	ν
76%	90%	10^{-8}	$(99.997 \pm 0.002)\%$

$D_{\alpha}^{k(m-i)} = C_k^{m-i} P_{\alpha}^{m-i} (1 - P_{\alpha})^{k-m+i}$ represents the sum of the probabilities of all possible cases where D_R detects $m - i$ out of k coherent states $|\alpha\rangle$ sent by Alice.

In addition, even if Bob obtains usable experimental results, D_R has a probability of clicking at the wrong time step, thus making him misjudge the elements in S . This requires us to define the correct probability $P(m, k) = P_{-\alpha}^m (1 - P_{\alpha})^k / E$ when the experimental results are available. Thus, the success probability is modified to $P_{\text{suc}} = E \times P(m, k)$. Based on the expectation of 100% success, the number of quantum samples required to complete the task is

$$R = \frac{n|\alpha|^2}{P_{\text{suc}}}. \quad (6)$$

Without loss of generality, we choose a special set S_j to verify the quantum advantage of our protocol, where $S_j = \{1, 2, \dots, j-1, j+1, \dots, n\}$ and size $k_j := |S_j| = n-1$. Therefore, the correct probability can be simplified as

$$P(1, n-1) = \frac{P_{-\alpha}(1 - P_{\alpha})^{n-1}}{D_{-\alpha}^{10} D_{\alpha}^{(n-1)1} + D_{-\alpha}^{11} D_{\alpha}^{(n-1)0}}. \quad (7)$$

Based on the above formulae, we present the numerical simulation in Fig. 2. The simulation results also guide our experimental demonstration. Figure 2a shows that a higher intensity results in a higher correct probability $P(1, n - 1)$. This is because D_R can more easily detect a higher intensity $|- \alpha \rangle_i$ sent by Alice. In contrast, as the visibility ν of the interferometer is not perfect, higher intensity also increases the probability of D_R clicking when Alice sends $|\alpha\rangle_i$. These two factors lead to the experimental efficiency E and success probability P_{suc} increasing first and then decreasing with an increase in light intensity. P_{suc} directly affects the number of quantum samples required to complete the task. Therefore, we must choose an appropriate light intensity to achieve a balanced trade-off between improving the correct probability and reducing quantum resources.

Figure 2b shows a comparison between the resources required by our protocol and the size of the set $[n]$ with the correct probability $P(1, n - 1) = 90\%$. To highlight our quantum advantage, we also draw the classical limit of the required samples for comparison. The cost of our protocol is lower than the classical limit when $n < 29,000$. When $n < 20,000$, the samples required by our protocol is less than half of that required by the classical protocols.

Note that the objective of this article was to construct a specific computational task for experimentally demonstrating quantum advantages in the context of machine learning and communication complexity. Therefore, to simplify the implementation of our protocol, we do not consider the case in which Alice sends incorrect coherent pulses to Bob. In fact, this case belongs to a more complex communication task and is beyond the scope of this

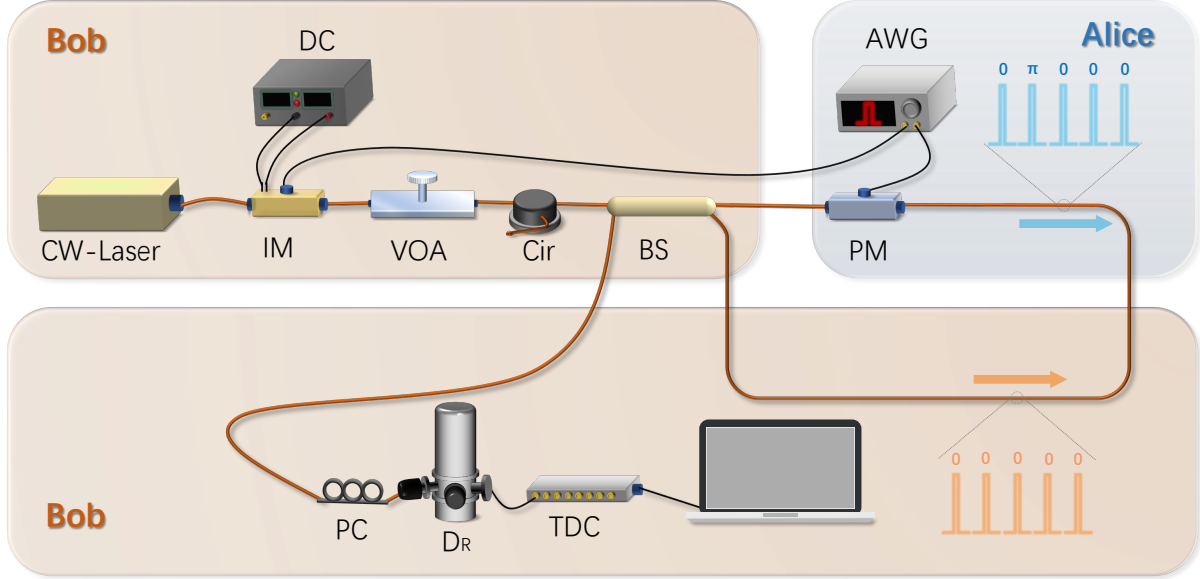


FIG. 3. Experimental set-up for the coherent-state quantum coupon collector protocol. The optical pulses were generated by a 1550.12 nm continuous-wave (CW) laser source with an intensity modulator (IM) driven by an external arbitrary waveform generator (AWG). The frequency of the pulse sequences and the duration of a single pulse were 312.5 MHz and 900 ps, respectively. These pulses were attenuated to the single-photon level by a variable optical attenuator (VOA), and then separated into two pulse sequences with different propagation directions by a 50 : 50 beam splitter (BS). The clockwise pulse sequence was set to $|\alpha, S\rangle$ after passing a phase modulator (PM) controlled by the AWG. The counterclockwise pulse sequence was used as the local state $|\alpha, [n]\rangle$. Finally, these two pulses interfered at the BS and were detected by a superconducting nanowire single-photon detector D_R . A polarisation controller (PC) was used to modify the polarisation of the incident pulses to achieve the maximum detection efficiency. The detection events were recorded using a time-to-digital converter (TDC).

article.

Experimental setup and results. We used linear optics components and single-photon detectors to present a proof-of-principle experimental demonstration of the coherent-state quantum coupon collector protocol (Fig. 3). First, the continuous-wave light with a wavelength of 1550.12 nm emitted by a laser source was carefully modulated into optical pulses at a repetition rate of 312.5 MHz by using an intensity modulator (IM). To make the modulated waveform as perfect as possible, the modulated light was monitored by a single photon detector instead of an oscilloscope during the modulation phase. Then, the modulated optical pulses were attenuated to the desired level by a variable optical attenuator (VOA) and separated by a 50 : 50 BS into two identical pulse sequences $|\alpha, [n]\rangle_A$ and $|\alpha, [n]\rangle_B$. These two pulse sequences travel clockwise and counterclockwise in the Sagnac loop. After passing through a phase modulator (PM), the clockwise pulse sequence $|\alpha, [n]\rangle_A$ is modulated to $|\alpha, S\rangle$ according to the value of the coupon S . To convert the counterclockwise sequence $|\alpha, [n]\rangle_B$ into the local state $|\alpha, [n]\rangle$, the PM is turned off when $|\alpha, [n]\rangle_B$ passes through it. We used the Sagnac loop to automatically stabilise the phase fluctuation of the channel to improve interference visibility. In addition, to make the two pulse sequences pass through the PM at different times, one arm of the Sagnac loop was designed to be 1 m longer

than the other arm. The optical circulator was used to prevent the previous optical pulses transmitted back by the BS from affecting the subsequent optical pulses. Finally, the interference results were detected using a superconducting nanowire single-photon detector (D_R).

Our scheme combines all copies of the $|S\rangle$ required to learn S into a sequence of n coherent states. Compared with a state that consists of a single photon in n modes, the coherent state sequence is easier to prepare. Moreover, combining all copies of $|S\rangle$ enhances the mean photon number of each time mode of the coherent state sequence, thus increasing the probability of measuring each mode. These features make our scheme easier to implement in experiments, and more effective.

Note that only if each element $i \in [n]$ is correctly classified as S or \bar{S} can we learn S correctly. Therefore, even if p_d and ν have a small effect on a single pulse, it is difficult to correctly classify all elements $i \in [n]$ when n is very large. This means that p_d and ν limit the maximum size of $[n]$ that our protocol can achieve quantum advantage with a given correct probability. However, in our experiment, because p_d can reach the order of 10^{-8} under the current experimental conditions, the effects of the random detection events caused by p_d can be ignored. In contrast, the maximum visibility of an interferometer ν that can be achieved in a laboratory is on the order of $1 - 10^{-5}$. As a result, ν seriously limits the success

TABLE II. Summary of the experimental data. The input size L ranges from 2,000 to 18,000 with a step size of 2,000. For each size L , we collected data for 5 seconds. The table shows the number of coupons sent, the number of detection events within the corresponding time windows, the number of events in which the detector clicked only once in each coupon period, the number of events in which the detector clicked only once and clicks at the correct time step, the correct probability; the efficiency, the success probability, the minimum number of classical samples required for classical protocols, the number of quantum samples needed to obtain the correct result utilised in our experiments.

L	μ	Total coupons	Detection events	Single clicks	Correct clicks	Correct probability	Efficiency	Success probability	Classical samples	Quantum samples
2000	1	781250	763766	525445	490824	93.4 %	67.2%	62.8 %	1.52×10^4	3.18×10^3
4000	2	390625	366475	254409	233479	91.7 %	65.1%	59.8 %	3.32×10^4	1.34×10^4
6000	2	260416	138071	120573	109603	90.4 %	46.3%	46.3 %	5.22×10^4	2.85×10^4
8000	3	195312	135981	104831	94767	90.4 %	53%	48.5 %	7.19×10^4	4.95×10^4
10000	3	156250	99214	82767	75900	91.7 %	53.0%	48.6 %	9.21×10^4	6.18×10^4
12000	4	130208	118189	79260	71477	90.1 %	60.8%	54.9 %	1.13×10^5	8.74×10^4
14000	5	111607	96421	68674	62797	91.4 %	58.6%	54.4 %	1.34×10^5	1.24×10^5
16000	6	97656	92380	64554	59817	92.6 %	66.1%	61.2 %	1.55×10^5	1.57×10^5
18000	7	86805	81783	57499	53706	93.4 %	59.2%	53.6 %	1.76×10^5	2.04×10^5

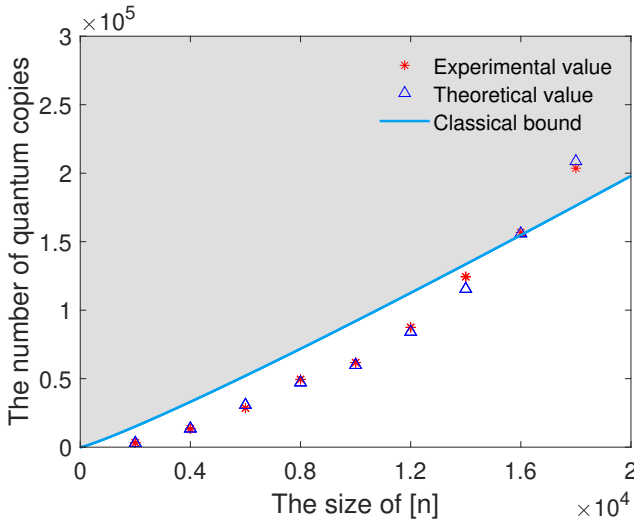


FIG. 4. Relationship between the required samples and the size of the set $[n]$. We compare the classical lower bound, the samples consumed by our protocol in the practical setup with the experimental parameters listed in Table I and its theoretically expected values. The experimental results were in line with the theoretically expected values. For an input size of under 14,000, our results outperformed the classical lower bound, thus demonstrating quantum advantage.

probability of learning S , even if the size of $[n]$ is relatively small. In addition, η directly affects the number of quantum samples required to complete the task. Therefore, ν and η are the experimental parameters that need to be improved. When the accuracy of ν is improved in the future, our protocol can also achieve quantum advantage over $[n]$ with a larger size.

To improve the success probability, we selected a BS whose visibility in the Sagnac loop was nearly 99.9993%. We also reduced the magnitude of the dark count probability p_d to 10^{-8} . At this magnitude, the dark count

probability hardly affects the system performance. In addition, we tried to adjust the amplitude of the radio-frequency signal driving the PM to achieve an accurate π -phase shift. However, it is almost impossible for a PM to apply a perfect π -phase shift on a specific pulse without influencing other pulses in a period, especially as the duty cycle in this experimental demonstration is on the order of $10^{-4} \sim 10^{-5}$. Consequently, the number of D_R clicks caused by the pulses $|\alpha\rangle_i$ in a coupon period is much higher than theoretically expected, which means that the experimental interference visibility is lower than that of the BS. Fortunately, during data processing, we found that selecting certain time windows can significantly improve the visibility for interference. However, this approach inevitably filters out certain detection events, thereby affecting the final success probability. By repeatedly selecting different time windows, we achieved a better trade-off between improving visibility and reducing detection events, thereby reducing the number of quantum samples of different coupon lengths.

The experiment was performed with different sizes of the set $[n]$ ranging from 2000 to 18000. For each size L , we ran the experiment for 5 s and analysed the detection results. The relevant experimental parameters are listed in Table I. The detailed results are listed in Table II. Our protocol consumes fewer samples than the classic protocol for $L < 16000$ (Fig. 4). The grey area in Fig. 4 indicates the region in which our protocol consumes more samples than the classical one. By choosing different time windows, we set $\nu = 0.99996$ for $n \leq 6000$ and $\nu = 0.99999$ for $n \geq 8000$. Note that these visibility levels are approximate values based on experimental data. To achieve better experimental results, we did not choose the time window with the most detection events, but the window with the highest visibility. The result is that only a fraction of the photons were detected, which is equivalent to reducing the detection efficiency of detector D_R . Therefore, the intensities of the coherent state

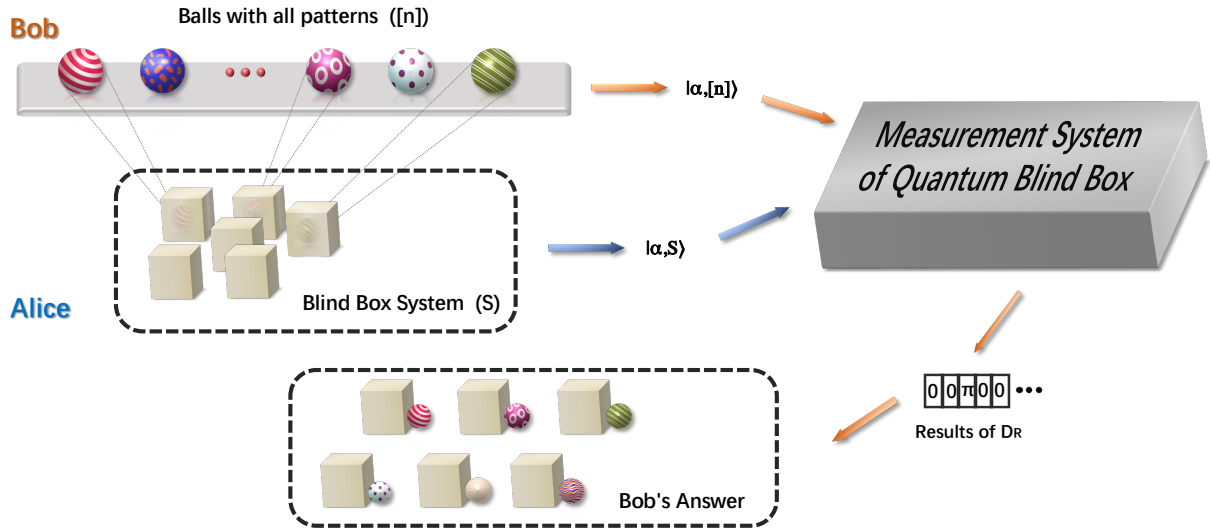


FIG. 5. Diagram of a quantum blind box. Alice prepares several balls with different patterns ($[\mathbf{n}]$). Alice then puts some of these balls into boxes to form a blind box system (S) and encodes them into a coherent state $|\alpha, S\rangle$. To determine the balls contained in Alice's blind box system, Bob encodes all balls into a local state $|\alpha, [\mathbf{n}]\rangle$. Alice generates $|\alpha, S\rangle$ and $|\alpha, [\mathbf{n}]\rangle$ in the measurement system of a quantum blind box, and Bob adjusts their total intensity in the system. Finally, Bob uses the results of D_R to determine which balls are included in Alice's blind box system.

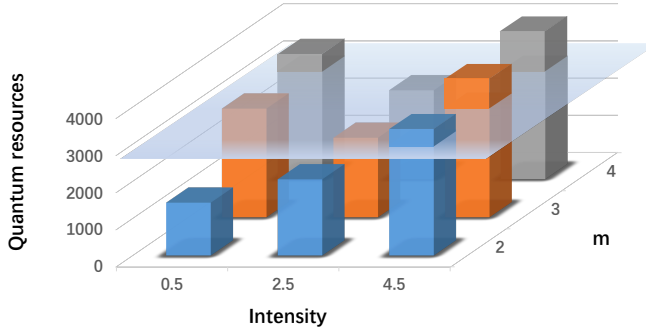


FIG. 6. Experimental results of the quantum blind box game. For m , we tested different values of m with a light intensity of 0.25, 0.5, 2.5, and 4.5. The Z-axis represents the expected value of the quantum resources that Bob spends to obtain the correct answer. The plane represents the classical limit. Note that for different m , the classical limit is different. Therefore, the plane is not strictly a plane, but it looks like a plane because the gap is too small. The quantum resources at certain light intensities do not exceed the plane, which means that Bob can use these light intensities to break the classical limit.

pulses were modulated much higher than theoretically expected in this experiment. Reducing the voltage fluctuations of the phase modulator and selecting a better time window can further improve the experimental results.

Quantum blind box. Our protocol can not only be used to verify quantum advantage in machine learning from the PAC theory, but also can be regarded as a communication task to demonstrate quantum advantage in

communication complexity. To this end, we designed a specific application scenario for our protocol, which is called a quantum blind box game. In this game (Fig. 5), Alice acts as a merchant, and Bob acts as a customer. Alice prepares n small balls with different patterns and packs them in boxes to form blind boxes. Alice then takes $n - m$ of these boxes as a blind box system, where $m \geq 1$, and encodes the coherent state $|\alpha, S\rangle$ according to the patterns of the balls in that system. Alice then tells Bob all patterns of the balls and the number of blind boxes in the blind box system.

To determine the patterns contained in the blind box system, Bob uses the same encoding method as Alice to create a local state $|\alpha, [n]\rangle$. The merchant Alice provides the entire measurement system, which is the same as the experimental device shown in Fig. 3. Bob can decide the total intensity μ of the coherent state $|\alpha, S\rangle$ sent by Alice, but the money he needs to pay to Alice is equal to the quantum resources consumed by $|\alpha, S\rangle$. The required quantum resources are $O(\mu \log_2 n)$ bits [29, 59]. Therefore, the higher the intensity μ of $|\alpha, S\rangle$, the more money Bob needs to pay. Finally, Bob judges the patterns in the blind box system based on the results of the single-photon detector D_R . If Bob gives the correct answer, he will be rewarded with $(n - m) \log_2(n - m) \log_2 n$ dollars, which is the minimum expected value of the information that needs to be transmitted to obtain the correct answer using classic resources. Therefore, when Bob consumes less quantum resources than the classical limit, he can obtain a positive return in this transaction.

Let us consider $n = 100$ and $m \in \{2, 3, 4\}$ as an example for demonstrating this game. The experimental results show that for a given value of m , the expected

TABLE III. Summary of notable quantum advantage demonstrations, with outlines of which fields the demonstrated quantum advantages belong to and the methods used to demonstrate them.

	Demonstrated quantum advantages			Methods	
	Communication complexity	Machine learning	Computational power		
This work	YES	YES	-		Linear Optics
Gong <i>et al.</i> (2021) [60]	-	-	YES	Superconducting Processor	
Centrone <i>et al.</i> (2021) [33]	YES	-	-	Linear Optics	
Zhong <i>et al.</i> (2020) [61]	-	-	YES	Linear Optics	
Arute <i>et al.</i> (2019) [27]	-	-	YES	Superconducting processor	
Kumar <i>et al.</i> (2019) [31]	YES	-	-	Linear Optics	
Arrazola <i>et al.</i> (2018) [32]	YES	-	-	Linear Optics	
Bravyi <i>et al.</i> (2018) [22]	-	-	YES	Quantum Circuits	
Boixo <i>et al.</i> (2018) [26]	-	-	YES	Quantum Circuits	
Neville <i>et al.</i> (2017) [14]	-	-	YES	Linear Optics	
Xu <i>et al.</i> (2015) [29]	YES	-	-	Linear Optics	
Bentivegna <i>et al.</i> (2015) [18]	-	-	YES	Integrated Photonic Circuits	
Broome <i>et al.</i> (2013) [15]	-	-	YES	Tunable Circuit	

quantum resources are significantly affected by the light intensity (Fig. 6). The detailed experimental results are presented in the Methods section. Note that the comparison used herein is the expected value of the quantum resources spent to obtain the correct answer. When the light intensity is small, Bob will not spend a large amount of resources in each game, but it is also difficult to obtain the correct answer. To obtain the bonus, Bob may need to play multiple games. As a result, the expected value of the quantum resources that he spends has increased. This is the reason why quantum resources at a 0.25 light intensity are relatively high for $m = 3$ and $m = 4$.

Figure 6 also shows that Bob can break the classical limit by choosing the proper intensity for achieving a positive return. In other words, Bob successfully uses quantum resources to design a better strategy than random extraction in this game. This means that in the quantum blind box game, Alice can also allow customers to design various coding methods and measurement strategies for guessing the blind box. The smaller the expected value of the information required for a strategy designed by a customer, the more he can get in return. Overall, quantum advantage in communication complexity has been successfully demonstrated in experiments through the quantum blind box game. We reasonably expect that the ideas contained in this game can be used to design communication protocols with a lower amount of information needed to complete specified communication tasks.

Discussion

Prior works have mainly demonstrated quantum advantages of improving the security of communication and enhancing computational power for specific tasks. Although there are many studies trying to find the superiority of quantum machine learning, these studies have not theoretically prove quantum advantages of machine learning. In this work, we propose a coherent-state quantum coupon collector protocol and demonstrate it experimentally by using simple linear optical elements and co-

herent states. Experimental results show that our protocol can effectively reduce the number of samples required to learn coupons exactly with up to 14000 elements on the basis of a 90% correct probability. Combined with the arguments in Ref. [49], our result strongly demonstrates quantum advantages of machine learning under current technology. To compare with quantum advantages achieved by other studies, we summarise them in Table. III. Note that our scheme does not resort to immature technologies, such as complicate entangled states or ideal single-photon sources. This makes our scheme particularly practical, especially for exemplifying the ability of linear optics.

Besides the demonstration of quantum advantage of machine learning based on the PAC learning theory for the first time, we also specially designed a quantum blind box game based on our protocol and experimentally demonstrated quantum advantage in communication complexity through this game. Our protocol does not save resources exponentially like other communication tasks with quantum advantages. Nevertheless, our protocol can still effectively learn the missing elements in the set $[n]$. We hope that the ideas contained in this game can inspire other useful applications, such as quantum voting.

Overall, despite potential limitations, our study provides new opportunities for the development of quantum machine learning and quantum communication complexity. We expect that the ability of linear optics can help us achieve more quantum-advantaged communication and computational schemes.

Methods

Selection of time windows. As described above, the visibility ν of the interferometer plays a crucial role in determining the cost in terms of quantum resources. Without phase modulation, ν in our scheme can easily reach over 99.999%. However, imperfections in PM often cause extra counts in unexpected places, which leads to a de-

TABLE IV. Experimental data of quantum blind box. We take $n = 100$ as an example and perform phase modulation on m places randomly, where $m \in \{2, 3, 4\}$. For $m \in \{2, 3, 4\}$, the classical resource consumptions are 2985.3, 2948.2, and 2911.2, respectively.

m	intensity	m	clicks	Correct clicks	Correct probability	Efficiency	Success probability	Quantum resources
2	0.5	119433	116560	97.6%	23.9%	23.3%	1425.0	
	2.5	407768	404469	99.2%	81.6%	80.9%	2053.3	
	4.5	433641	431329	99.5%	86.7%	86.2%	3465.7	
3	0.5	58772	56692	96.5%	11.7%	11.3%	2929.8	
	2.5	392690	387474	98.7%	78.5%	77.5%	2143.3	
	4.5	403131	397836	98.7%	80.6%	79.5%	3757.5	
4	0.5	25900	24570	94.9%	5.2%	4.9%	3380.0	
	2.5	353685	347275	98.2%	77.1%	76.5%	2391.4	
	4.5	379154	372500	98.2%	85.6%	85.1%	4013.1	

crease in visibility.

Fortunately, we find that the visibility varies when different time windows are chosen, which is why the simulation shown in Fig. 4 uses two visibilities. The choice of time window also affects the number of detection events. In our experiment, as visibility increased, the number of detected events tended to decrease, which is equivalent to a decrease in the detection efficiency. Therefore, the equivalent detection efficiencies and visibilities for different time windows are different.

To ensure the correct probability $P(m, k) > 90\%$, we traverse different time windows to find the minimum value of the expected value of the required quantum resources. For the expected values displayed shown in Fig. 4, we adapted the corresponding experimental parameters according to the time window.

Experimental details of quantum blind box. In the experiment, we correlate the patterns of the balls to the positions of the pulses. The corresponding positions of the balls that are not in the blind box system are loaded with a π -phase. Therefore, this game can be realised

using the experimental setup shown in Fig. 3.

The system was run at a repetition rate of 10 MHz, and each round was 5 seconds long. The duty cycle of a pulse was about 5%. The dark count rate per 5 ns detection gate was approximately 6×10^{-7} . Considering the channel loss, the detection efficiency was approximately 68%. The detailed experimental results are presented in Table IV. The experimental apparatus was the same as used before.

Acknowledgements

We gratefully acknowledge the support from the National Natural Science Foundation of China (No. 61801420), the Natural Science Foundation of Jiangsu Province (No. BK20211145), the Fundamental Research Funds for the Central Universities (No. 020414380182), the Key Research and Development Program of Nanjing Jiangbei New Aera (No. ZDYD20210101), the Key-Area Research and Development Program of Guangdong Province (No. 2020B0303040001) and the China Postdoctoral Science Foundation (No. 2021M691536).

[1] Pappa, A. *et al.* Experimental plug and play quantum coin flipping. *Nat. Commun.* **5**, 3717 (2014).

[2] Xu, F., Ma, X., Zhang, Q., Lo, H.-K. & Pan, J.-W. Secure quantum key distribution with realistic devices. *Reviews of Modern Physics* **92**, 025002 (2020).

[3] Liu, W.-B. *et al.* Homodyne detection quadrature phase shift keying continuous-variable quantum key distribution with high excess noise tolerance. *PRX Quantum* **2**, 040334 (2021).

[4] Lunghi, T. *et al.* Experimental bit commitment based on quantum communication and special relativity. *Phys. Rev. Lett.* **111**, 180504 (2013).

[5] Fu, Y., Yin, H.-L., Chen, T.-Y. & Chen, Z.-B. Long-distance measurement-device-independent multi-party quantum communication. *Phys. Rev. Lett.* **114**, 090501 (2015).

[6] Zhang, W. *et al.* Quantum secure direct communication with quantum memory. *Phys. Rev. Lett.* **118**, 220501 (2017).

[7] Lucamarini, M., Yuan, Z. L., Dynes, J. F. & Shields, A. J. Overcoming the rate-distance limit of quantum key distribution without quantum repeaters. *Nature* **557**, 400–403 (2018).

[8] Yin, H.-L., Fu, Y. & Chen, Z.-B. Practical quantum digital signature. *Phys. Rev. A* **93**, 032316 (2016).

[9] Barz, S. *et al.* Demonstration of blind quantum computing. *Science* **335**, 303–308 (2012).

[10] Gu, J. *et al.* Secure quantum secret sharing without signal disturbance monitoring. *Opt. Express* **29**, 32244–32255 (2021).

[11] Alikhani, P. *et al.* Experimental relativistic zero-knowledge proofs. *Nature* **599**, 47–50 (2021).

[12] Li, Z. *et al.* Finite-key analysis for quantum conference key agreement with asymmetric channels. *Quantum Sci.*

Technol. **6**, 045019 (2021).

[13] Aaronson, S. & Arkhipov, A. The computational complexity of linear optics. In *Proceedings of the forty-third annual ACM symposium on Theory of computing*, 333–342 (2011).

[14] Neville, A. *et al.* Classical Boson sampling algorithms with superior performance to near-term experiments. *Nat. Phys.* **13**, 1153–1157 (2017).

[15] Broome, M. A. *et al.* Photonic Boson sampling in a tunable circuit. *Science* **339**, 794–798 (2013).

[16] Tillmann, M. *et al.* Experimental Boson sampling. *Nat. Photon.* **7**, 540–544 (2013).

[17] Crespi, A. *et al.* Integrated multimode interferometers with arbitrary designs for photonic Boson sampling. *Nat. Photon.* **7**, 545–549 (2013).

[18] Bentivegna, M. *et al.* Experimental scattershot Boson sampling. *Sci. Adv.* **1**, e1400255 (2015).

[19] Zhong, H.-S. *et al.* Experimental gaussian Boson sampling. *Sci. Bull.* **64**, 511–515 (2019).

[20] Farhi, E. & Harrow, A. W. Quantum supremacy through the quantum approximate optimization algorithm. *arXiv preprint arXiv:1602.07674* (2016).

[21] Bremner, M. J., Montanaro, A. & Shepherd, D. J. Achieving quantum supremacy with sparse and noisy commuting quantum computations. *Quantum* **1**, 8 (2017).

[22] Bravyi, S., Gosset, D. & König, R. Quantum advantage with shallow circuits. *Science* **362**, 308–311 (2018).

[23] Gao, X., Wang, S.-T. & Duan, L.-M. Quantum supremacy for simulating a translation-invariant Ising spin model. *Phys. Rev. Lett.* **118**, 040502 (2017).

[24] Bermejo-Vega, J., Hangleiter, D., Schwarz, M., Raussendorf, R. & Eisert, J. Architectures for quantum simulation showing a quantum speedup. *Phys. Rev. X* **8**, 021010 (2018).

[25] Aaronson, S. & Chen, L. Complexity-theoretic foundations of quantum supremacy experiments. *arXiv preprint arXiv:1612.05903* (2016).

[26] Boixo, S. *et al.* Characterizing quantum supremacy in near-term devices. *Nat. Phys.* **14**, 595–600 (2018).

[27] Arute, F. *et al.* Quantum supremacy using a programmable superconducting processor. *Nature* **574**, 505–510 (2019).

[28] Horn, R. T., Babichev, S., Marzlin, K.-P., Lvovsky, A. & Sanders, B. C. Single-qubit optical quantum fingerprinting. *Phys. Rev. Lett.* **95**, 150502 (2005).

[29] Xu, F. *et al.* Experimental quantum fingerprinting with weak coherent pulses. *Nat. Commun.* **6**, 8735 (2015).

[30] Guan, J.-Y. *et al.* Observation of quantum fingerprinting beating the classical limit. *Phys. Rev. Lett.* **116**, 240502 (2016).

[31] Kumar, N., Kerenidis, I. & Diamanti, E. Experimental demonstration of quantum advantage for one-way communication complexity surpassing best-known classical protocol. *Nat. Commun.* **10**, 4152 (2019).

[32] Arrazola, J. M., Diamanti, E. & Kerenidis, I. Quantum superiority for verifying NP-complete problems with linear optics. *npj Quant. Inform.* **4**, 56 (2018).

[33] Centrone, F., Kumar, N., Diamanti, E. & Kerenidis, I. Experimental demonstration of quantum advantage for NP verification with limited information. *Nat. Commun.* **12**, 850 (2021).

[34] Goodfellow, I., Bengio, Y. & Courville, A. *Deep learning* (MIT Press, Cambridge, Mass., 2016).

[35] Biamonte, J. *et al.* Quantum machine learning. *Nature* **549**, 195–202 (2017).

[36] Bondarenko, D. & Feldmann, P. Quantum autoencoders to denoise quantum data. *Phys. Rev. Lett.* **124**, 130502 (2020).

[37] Cong, I., Choi, S. & Lukin, M. D. Quantum convolutional neural networks. *Nature Physics* **15**, 1273–1278 (2019).

[38] Beer, K. *et al.* Training deep quantum neural networks. *Nat. Commun.* **11**, 808 (2020).

[39] Chen, Z.-B. Quantum neural network and soft quantum computing. *arXiv preprint arXiv:1810.05025* (2018).

[40] Schuld, M., Sinayskiy, I. & Petruccione, F. The quest for a quantum neural network. *Quantum Inf. Process.* **13**, 2567–2586 (2014).

[41] Lewenstein, M. Quantum perceptrons. *J. Mod. Opt.* **41**, 2491–2501 (1994).

[42] Wan, K. H., Dahlsten, O., Kristjánsson, H., Gardner, R. & Kim, M. Quantum generalisation of feedforward neural networks. *npj Quant. Inform.* **3**, 36 (2017).

[43] da Silva, A. J., Ludermir, T. B. & de Oliveira, W. R. Quantum perceptron over a field and neural network architecture selection in a quantum computer. *Neural Netw.* **76**, 55–64 (2016).

[44] Killoran, N. *et al.* Continuous-variable quantum neural networks. *Phys. Rev. Research* **1**, 033063 (2019).

[45] Torrontegui, E. & García-Ripoll, J. J. Unitary quantum perceptron as efficient universal approximator. *Europhys. Lett.* **125**, 30004 (2019).

[46] Arrazola, J. M. *et al.* Machine learning method for state preparation and gate synthesis on photonic quantum computers. *Quantum Sci. Technol.* **4**, 024004 (2019).

[47] Valiant, L. G. A theory of the learnable. *Communications of the ACM* **27**, 1134–1142 (1984).

[48] Haussler, D. *Probably approximately correct learning* (University of California, Santa Cruz, Computer Research Laboratory, 1990).

[49] Arunachalam, S. *et al.* Quantum coupon collector. In *15th Conference on the Theory of Quantum Computation, Communication and Cryptography* (2020).

[50] Motwani, R. & Raghavan, P. *Randomized algorithms* (Chapman & Hall/CRC, 2010).

[51] Du, J. *et al.* Experimental quantum multimeter and one-qubit fingerprinting. *Phys. Rev. A* **74**, 042319 (2006).

[52] de Beaudrap, J. N. One-qubit fingerprinting schemes. *Phys. Rev. A* **69**, 022307 (2004).

[53] Brassard, G. Quantum communication complexity. *Found. Phys.* **33**, 1593–1616 (2003).

[54] Steane, A. M., van Dam, W. *et al.* Physicists triumph at guess my number. *Phys. Today* **53**, 35–39 (2000).

[55] Buhrman, H., Cleve, R., Massar, S. & De Wolf, R. Non-locality and communication complexity. *Rev. Mod. Phys.* **82**, 665 (2010).

[56] Kushilevitz, E. *Communication complexity*. vol. 44 (Cambridge Univ. Press, 2006).

[57] Massar, S. Quantum fingerprinting with a single particle. *Phys. Rev. A* **71**, 012310 (2005).

[58] Garcia-Escartin, J. C. & Chamorro-Posada, P. Swap test and Hong-Ou-Mandel effect are equivalent. *Phys. Rev. A* **87**, 052330 (2013).

[59] Arrazola, J. M. & Lütkenhaus, N. Quantum fingerprinting with coherent states and a constant mean number of photons. *Phys. Rev. A* **89**, 062305 (2014).

[60] Gong, M. *et al.* Quantum walks on a programmable two-dimensional 62-qubit superconducting processor. *Science*

372, 948–952 (2021).

[61] Zhong, H.-S. *et al.* Quantum computational advantage using photons. *Science* **370**, 1460–1463 (2020).